Atmos. Meas. Tech., 5, 1425–1441, 2012
www.atmos-meas-tech.net/5/1425/2012/
doi:10.5194/amt-5-1425-2012
© Author(s) 2012. CC Attribution 3.0 License.

Atmospheric Measurement Techniques

Long-term validation of tropospheric column-averaged CH_4 mole fractions obtained by mid-infrared ground-based FTIR spectrometry

E. Sepúlveda[1,2], M. Schneider[2,3], F. Hase[3], O. E. García[2], A. Gomez-Pelaez[2], S. Dohe[3], T. Blumenstock[3], and J. C. Guerra[1]

[1]La Laguna University, Physics Department, Tenerife, Spain
[2]Izaña Atmospheric Research Center, Agencia Estatal de Meteorología (AEMET), Spain
[3]Institute for Meteorology and Climate Research (IMK-ASF), Karlsruhe Institute of Technology, Germany

Correspondence to: E. Sepúlveda (esepulvedah@aemet.es)

Received: 26 December 2011 – Published in Atmos. Meas. Tech. Discuss.: 13 February 2012
Revised: 25 May 2012 – Accepted: 29 May 2012 – Published: 26 June 2012

Abstract. At the Izaña Atmospheric Research Center, high-resolution mid-infrared solar absorption spectra have been recorded for more than 12 yr using Fourier Transform InfraRed (FTIR) spectrometers. We use the spectral fitting algorithm PROFFIT to retrieve long-term time series of methane (CH_4) from the measured spectra. We investigate the total column-averaged dry air mole fractions of methane ($totXCH_4$) obtained from a profile scaling and a profile retrieval, and apply two approaches for deriving the tropospheric column-averaged dry air mole fractions: firstly, we use the FTIR hydrogen fluoride (HF) total column amounts as an estimator for the stratospheric CH_4 contribution and a posteriori correct the $totXCH_4$ data of a profile scaling retrieval accordingly ($troXCH_{4_{post}}$); secondly, we directly determine the tropospheric column-averaged dry air mole fractions of methane ($troXCH_{4_{retr}}$) from retrieved CH_4 profiles. Our theoretical estimation indicates that the scaling retrieval leads to $totXCH_4$ amounts that are subject to a large smoothing error, which can be widely avoided by applying a profile retrieval (for the latter we estimate an overall precision of 0.41 %).

We compare the different FTIR CH_4 data to Izaña's Global Atmospheric Watch (GAW) surface in-situ CH_4 data ($CH_{4_{GAW}}$), which in the case of the Izaña Atmospheric Research Center high mountain observatory are very representative for the free tropospheric CH_4 amounts. Concerning $totXCH_4$, the agreement between the FTIR data product and the in-situ measurement is rather poor documenting that $totXCH_4$ is not a valid free tropospheric CH_4 proxy, as it is significantly affected by the varying stratospheric CH_4 contribution and it rather follows the variation in the tropopause altitude. The a posteriori correction method as applied here only removes a part of this stratospheric CH_4 contribution. In contrast the profile retrieval allows for a direct estimation of the tropospheric column-averaged CH_4 amounts. Results of the profile retrieval analysis correlate well with the $CH_{4_{GAW}}$ data (correlation coefficient of 0.60, FTIR-GAW scatter of 0.97 %), and both data sets show very similar annual cycles and trend behaviour for the 2001–2010 time period. Furthermore, we find a very good absolute agreement between the $troXCH_{4_{retr}}$ and $CH_{4_{GAW}}$ (mid-infrared FTIR/GAW scaling factor of 0.9987) suggesting that mid-infrared FTIR data can be well combined with the surface in-situ GAW data.

Our study strongly supports the value of mid-infrared ground-based FTIR CH_4 profile retrievals as well as the robustness of the approach for achieving total and tropospheric column-averaged XCH_4 data of high quality.

1 Introduction

Methane (CH_4) is the second most important anthropogenic greenhouse gas (GHG), after carbon dioxide (CO_2). While CH_4 is 200 times less abundant than CO_2, it is about 20 times more efficient than CO_2 to trap outgoing long wave radiation, on a 50 yr timescale. The change in the CH_4 mixing ratio

since pre-industrial times (1750) to 2005 (from 715 to 1774 ppb) gives a radiative forcing (RF) of $+0.48 \pm 0.05\,W\,m^{-2}$, ranking CH_4 as the second highest RF of the GHGs after CO_2 (RF of CO_2 in 2005, $1.66 \pm 0.17\,W\,m^{-2}$; IPCC, 2007). In 2009 CH_4 global atmospheric concentrations have reached more than 1780 ppb for column-averaged mole fractions on global average in 2009 (Frankenberg et al., 2011). At surface stations higher annual average values are registered (e.g. 1830 ppb at the Izaña's Global Atmospheric Watch (GAW) station in 2009, Gomez-Pelaez et al., 2010.

CH_4 plays an important role in atmospheric chemistry, affecting the oxidizing capacity of the atmosphere and acting as a precursor of tropospheric ozone (O_3). The main sources producing methane are considered to be biogenic CH_4 formation that occurs in natural wetlands, water-flooded rice paddies, landfills, stomachs of ruminant animals, incomplete burning of biomass, oceans and vegetation. Further sources are released from melting permafrost and from shallow hydrates on the continental shelf (Dlugokencky et al., 2009). Thermogenic formation is the main process for generation of natural gas deposits over geological time scales. Parts of this inventory are released into the atmosphere due to fossil fuel extraction, processing, transportation and distribution (Keppler et al., 2006; Frankenberg et al., 2005). The main sink of atmospheric CH_4 is the reaction with hydroxyl radical OH. The destruction of CH_4 by OH in the troposphere represents about 90 % of CH_4 loss in the atmosphere. The rest of the sink is due to an uptake of CH_4 by soils, reaction with Cl in the marine boundary layer, and due to transport into the stratosphere where it is decomposed by reactions with OH, $O(^1D)$ and Cl (Bousquet et al., 2011).

Prediction of the evolution of GHGs in the atmosphere requires an understanding of their sources and sinks. Therefore, inverse modelling techniques applying atmospheric concentration measurement monitored at global surface networks are used (Bousquet et al., 2011). The in-situ surface measurements show very high precision and absolute accuracy (approx. 0.1 %), but they are strongly affected by local processes like small-scale turbulences or nearby sources or sinks. It is very difficult for the inverse models to capture these small-scale processes. In this context, vertically averaging the concentrations can be helpful. For instance, Olsen and Randerson (2004) document that total column-averaged observations of GHGs are significantly less affected by small-scale processes, but still conserve valuable GHG source/sink information. However, total column-averaged data are affected by the stratospheric contribution, the correct modelling of which is a significant error source when investigating the GHG cycling between the atmosphere, the biosphere, and the ocean.

Ground-based high spectral resolution FTIR measurements allow a precise determination of the atmospheric abundances (total column amounts and vertical profiles) of many constituents, including GHGs. The ground-based FTIR total column data are essential for the validation of GHGs measured from space by current and future satellite sensors (e.g. SCIAMACHY, GOSAT, OCO-2). Furthermore, by means of the ground-based FTIR vertical profile data, one can calculate tropospheric column-averaged mixing ratios. These ratios would neither be affected by small-scale near-surface processes nor by stratospheric contributions. If provided with high accuracy and precision, the tropospheric column-averaged mixing ratios would be a very useful data product for investigating the GHG cycling between the atmosphere, the biosphere, and the ocean.

In this work we present, discuss, and validate different ground-based FTIR CH_4 products derived from mid-infrared spectral region: the total column-averaged volume mixing ratio ($totXCH_4$), and two tropospheric column-averaged volume mixing ratios ($troXCH_4$): a first derived by a posteriori correction method using HF as indicator for the stratospheric contribution (similar to Washenfelder et al., 2003), and a second directly retrieved from the measured spectra.

In the following Sect. 2, we describe the CH_4 program at the Izaña Atmospheric Research Center: the GAW in-situ and FTIR activities. In Sect. 3 we present the FTIR technique and the FTIR CH_4 products. We describe the data analysis method and document the characteristics of the FTIR data (sensitivity and uncertainty). In Sect. 4 the different FTIR CH_4 products are compared to the GAW surface CH_4 measurements. In Sect. 5 we comment on the comparability of retrievals in the mid- and near- infrared spectral region, and Sect. 6 summarizes our study.

2 CH_4 program at the Izaña Atmospheric Research Center

2.1 Site description

Izaña is a subtropical high mountain observatory located on the Canary Island of Tenerife, 300 km from the African west coast at 28°18′ N, 16°29′ W at 2370 m a.s.l. It is part of the Meteorological State Agency of Spain (Spanish acronym: AEMET), and it is run by the Izaña Atmospheric Research Center. It is a global station of the WMO (World Meteorological Organisation) network of GAW (Global Atmospheric Watch) stations and has a comprehensive measurement program of a large variety of different atmospheric constituents. More detailed information can be found on the official webpage of the Izaña Atmospheric Research Center: http://www.izana.org.

The Izaña Observatory is usually located above a strong subtropical temperature inversion layer (generally well established between 500 and 1500 m a.s.l.). While during daytime the strong diurnal insolation generates a slight upslope flow of air originating from below the inversion layer (from a woodland that surrounds the station at a lower altitude), during nighttime the Izaña Observatory is very representative of the free troposphere (or at least of the lower levels of the free troposphere; see Fig. 1).

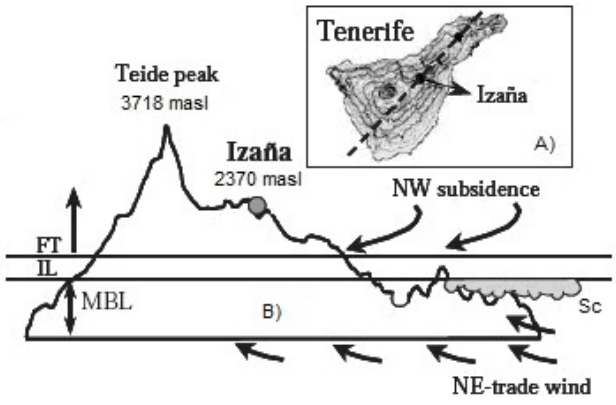

Fig. 1. (A) Location of Izaña in Tenerife Island, **(B)** transect of Tenerife Island – along the dotted line in **(A)** – showing the vertical stratification: MBL: marine boundary layer, IL: inversion layer, FT: free troposphere, Sc: stratocumulus.

2.2 In-situ measurement program

Continuous surface in-situ measurements of atmospheric CO_2 and CH_4 have been carried out at Izaña station since 1984. Furthermore, CO concentrations have been measured since 1998 and N_2O and SF_6 since 2007.

CH_4 mole fraction is measured using a DANI 3800 gas chromatograph. The carrier gas is synthetic air. Ambient air is cooled to $-70\,^{\circ}C$ to partially remove water vapour content before flowing towards the sample loop (10 ml size). Sample loop temperature is not regulated. A self-developed software integrator provides the area and height of the CH_4 peak in the chromatogram. See Gomez-Pelaez and Ramos (2011), and references therein, for more details about the measurements and technique. The most recent World Calibration Centre (WCC-Empa) system and performance audit for CH_4 at Izaña was carried in 2009 and documents the good quality of the Izaña CH_4 in-situ data (Zellweger et al., 2009). This good data quality is also confirmed by the continuous comparison to NOAA data obtained from simultaneously collected weekly flask samples (Gomez-Pelaez et al., 2012).

2.3 FTIR measurement program

Ground-based FTIR activities started at Izaña Observatory in the late 1990s in the framework of a collaboration between AEMET and KIT (Karlsruhe Institute of Technology, Germany). In 1999 KIT scientists installed a Bruker IFS 120M instrument at Izaña. In early 2005 KIT substituted this spectrometer by a Bruker IFS 125HR. During March–April of 2005, both instruments were running side-by-side. The Izaña FTIR experiment is involved in two global networks: since 1999 it has contributed to the Network for the Detection of Atmospheric Composition Change (NDACC, http://www.ndacc.org) and since 2007 to the Total Carbon Column Observing Network (TCCON, http://www.tccon.caltech.edu). For NDACC, solar absorption spectra are measured in the mid-infrared spectral region (740–4250 cm^{-1}, corresponding to 13.5–2.4 µm) and for TCCON in the near- infrared spectral region (3500–14 000 cm^{-1}, corresponding to 2.9–0.7 µm). The applied high-resolution FTIR spectrometer allows for a detailed observation of the pressure broadening effect, i.e. the absorption line width of an atmospheric absorber depends on the pressure (and thus altitude) where the absorption takes place. Therefore, one can retrieve concentration profiles of the atmospheric absorbers in addition to total column abundances. The Instrumental Line Shape (ILS) also affects the observed line shape, and in particular for the profile retrievals a continuous monitoring of the ILS is important. At Izaña we determine the ILS about every 2 months by low-pressure gas cell (HBr and N_2O) measurements and the LINEFIT software (LINEFIT code, Hase et al., 1999). The respective LINEFIT results are then applied in the atmospheric retrievals.

CH_4 has absorption lines in both the mid-infrared and near-infrared spectral regions. In this study we present CH_4 retrieved only from NDACC mid-infrared spectra.

3 Ground-based FTIR technique and CH_4 products

3.1 General setup of a ground-based FTIR analysis

Ground-based NDACC FTIR systems measure solar absorption spectra, under clear sky conditions, applying a high-resolution Fourier Transform Spectrometer (typical resolution of 0.005 cm^{-1}; maximum optical path difference, OPD_{max} of 180 cm). The measured spectra are simulated by a precise line-by-line radiative transfer model that applies the parameters of a spectroscopic database (e.g. HITRAN, Rothman et al., 2009). The basic equation for analyzing the solar absorption is the Lambert Beer's law:

$$I(\lambda) = I_{\text{sun}}(\lambda) \cdot \exp\left(-\int_{\text{TOA}}^{\text{Obs}} \sigma_x(\lambda, s(T,p)) \cdot x(s)\,\mathrm{d}s\right) \quad (1)$$

where $I(\lambda)$ is the measured intensity at wavelength λ, I_{sun} the extraterrestrial solar intensity, $\sigma_x(\lambda, s)$ is the absorption cross section and $x(s)$ the concentration of an absorber x at location s. The integration is performed along the path of the direct sunlight (between the Observer, Obs, and the Top Of the Atmosphere, TOA). At higher wavenumbers (above 1500 cm^{-1}), atmospheric self-emission can be neglected as compared to direct solar radiances.

For the purpose of numerical handling, the atmospheric state $x(s)$ and the simulated spectrum $I(\lambda)$ are discretized in form of a state vector $\boldsymbol{x}$ and a measurement vector $\boldsymbol{y}$. The measurement and state vector are related by a vector valued function $\boldsymbol{F}$, which simulates the atmospheric radiative transfer and the characteristics of the measurement system (spectral resolution, instrumental line shape, etc.): $\boldsymbol{y} = \boldsymbol{F}(\boldsymbol{x})$.

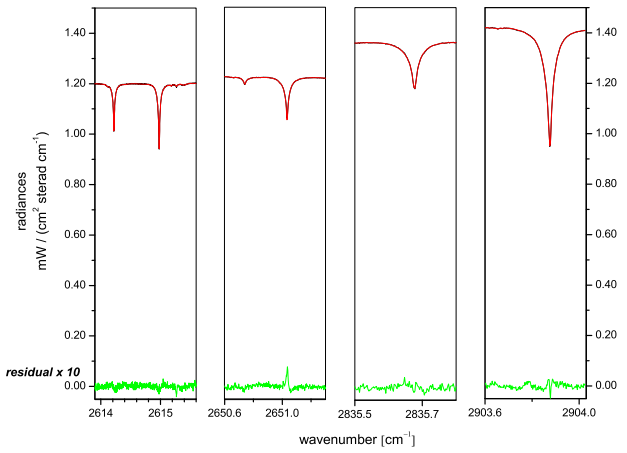

Fig. 2. The four applied spectral microwindows: measured spectrum (black), simulated spectrum (red), and residuals multiplied by a factor of 10 (green).

The derivatives $\partial \boldsymbol{y}/\partial \boldsymbol{x}$ determine the changes in the modelled spectral fluxes $\boldsymbol{y}$ for changes in the vertical distribution of the absorber $\boldsymbol{x}$. These derivatives are collected in a Jacobian matrix $\mathbf{K}$:$\partial \boldsymbol{y} = \mathbf{K}\partial \boldsymbol{x}$. Direct inversion of this last equation would allow an iterative calculation of the sought variables $\boldsymbol{x}$. However, the problem is generally ill-determined, i.e. the columns of $\mathbf{K}$ are not linearly independent and there are many solutions that are in acceptable agreement with the measurement. Thus, the solution has to be properly constrained. An extensive treatment of this topic is given in the textbook of C. D. Rodgers (Rodgers, 2000). We apply the retrieval code PROFFIT and the included radiative transfer code PROFFWD to accomplish our analysis (Hase et al., 2004).

3.2 The CH_4 retrieval strategy

Currently, the establishment of an improved NDACC CH_4 retrieval guideline is under discussion. The objective is an NDACC CH_4 product that approaches the high precision requirements of TCCON (a few per mil). At some stations NDACC measurements have been performed since the early 1990s, and high quality NDACC CH_4 data could well complement the TCCON time series, which are limited to the last few years.

Our CH_4 retrieval strategy is a modification of the current official NDACC retrieval guideline and includes a set of 4 microwindows containing strong, unsaturated, and isolated CH_4 lines (see Fig. 2 and Table 1). Besides CH_4 we have considered spectroscopic signatures of 7 interfering species. For the target species (CH_4) and the interfering species (CO_2, O_3, N_2O, NO_2 and HCl), we have applied spectroscopic parameters from HITRAN 2008 (Rothman et al., 2009), while for H_2O and OCS we have applied the recent HITRAN 2009 update.

As a-priori profiles of the interfering species, we apply the climatological entries from WACCM (The Whole Atmosphere Community Climate Model) provided by NCAR (National Centre for Atmospheric Research, J. Hannigan, personal communication, 2009). For the minor interfering species (O_3, N_2O, HCl and OCS), we simply simulate the spectral signatures according to the WACCM concentrations. For the major absorbers (CO_2 and NO_2), we scale the WACCM profiles during the CH_4 retrieval process and the H_2O interferences are accounted for by a two step strategy: first, we perform a dedicated H_2O retrieval (Schneider et al., 2010a) and then we scale the retrieved daily mean H_2O profile in the subsequent CH_4 retrieval process. Thereby, we minimise the interferences due to H_2O and HDO. Such interferences have been investigated in recent studies applying different sets of microwindows at both high and low altitude sites (Sussmann et al., 2011; Hase, 2011). Izaña is a rather dry high-altitude site, so the H_2O interference problem is less severe than for low latitude sites at sea-level. We expect that our results are transferable to at least other high altitude or polar sites of the NDACC.

Furthermore, we fit the continuum background slope and the residual ILS asymmetry. We use the NCEP analysis (National Centers for Environmental Prediction) at 12:00 UT as the temperature and pressure input profiles.

We examine two different CH_4 fitting procedures. A first consists in scaling the CH_4 WACCM a-priori profile (in the following referred to as scaling retrieval, SR), and a second retrieves CH_4 profiles (profile retrieval, PR), whereby a Tikhonov-Phillips method on a logarithmic scale is applied (Hase, 2000; Hase et al., 2004; Schneider et al., 2006).

3.3 The FTIR CH_4 products

3.3.1 Total column-averaged CH_4 dry air mole fraction (totXCH_4)

The totXCH_4 is calculated dividing the CH_4 total column by the dry pressure column (DPC) above Izaña. The DPC is calculated converting the ground pressure to column air concentration:

$$\mathrm{DPC} = \frac{P_s}{m_{\mathrm{dryair}} \cdot g\,(\varphi)} - \frac{m_{H_2O}}{m_{\mathrm{dryair}}} \times H_2O_{\mathrm{col}} \qquad (2)$$

being P_s the surface pressure at Izaña ground level, m_{dryair} the molecular mass of the dry air ($\sim$28.96 g mol^{-1}), m_{H_2O} the molecular mass of the water vapour ($\sim$18 g mol^{-1}), H_2O_{col} the water vapour total column amount (retrieved with a dedicated H_2O retrieval, Schneider, et al., 2010b), and $g(\varphi)$ the latitude-dependent surface acceleration due to gravity. The ground pressure was acquired with a Setra System (precision of $\pm$0.3 hPa).

Table 1. Spectral microwindows (MW) chosen for the CH_4 retrieval shown in this study.

	Spectral microwindows (cm^{-1})
MW1	2613.7000–2615.4000
MW2	2650.6000–2651.3000
MW3	2835.5000–2835.8000
MW4	2903.6000–2904.0250

3.3.2 A posteriori-corrected total column-averaged CH_4 dry air mole fraction ($troXCH_{4_{post}}$)

Similar to Washenfelder et al. (2003), we calculate the $troXCH_{4_{post}}$ from the CH_4 total column after correcting the variation in both surface pressure and stratospheric contribution:

$$troXCH_{4_{post}} = \frac{CH_{4_{col}} - b \cdot HF_{col}}{DPC} \quad (3)$$

where $CH_{4_{col}}$ is the CH_4 total column from the scaling retrieval, HF_{col} is the HF total column, and b is the stratospheric slope equilibrium relationship between the CH_4 and HF columns. In Appendix A we describe and discuss different approaches for calculating the b-value in the context of the method presented by Washenfelder et al. (2003).

In Eq. (3) we apply a de-trended HF total column time series retrieved from the FTIR measurements at Izaña. The HF trend and annual cycle were calculated by fitting the following function to the HF daily mean time series:

$$f(t) = a_1 + a_2 t + \sum_{j=1}^{2} \left[d_j \cos(k_j t) + e_j \sin(k_j t) \right] \quad (4)$$

where t is the time in days, a_1 is a constant value, a_2 is the parameter of the linear trend, and d_j and e_j are the parameters of the annual cycle ($k_j = 2\pi j/T$ with $T = 365.25$ days).

Subtracting $a_2 t$ from the HF time series yields the de-trended HF time series. Alternatively, we can divide the HF time series by the term $(a_1 + a_2 t)$, which yields a normalised and de-trended HF time series. The normalisation has the advantage that we can apply a normalised b-value, which does not change with a trend in HF (see discussion in Appendix A). Both the de-trended and normalised HF time series keep the variability caused by changes of the tropopause altitude (as long as there is no linear trend in the tropopause altitude), but are not affected by the anthropogenic HF increase. HF is believed to originate in the middle atmosphere solely from the photodissociation of man-made chlorofluorocarbons (CFCs) and hydrochlorofluorocarbons (HCFCs). The de-trending is performed in order to reduce the influence of the chemical variability of HF in the calculations. But it must be said that the whole HF chemical variability cannot be removed by de-trending. Finally, the variable fluorine partitioning between HF and COF_2 introduces additional uncertainty into the HF post-correction approach.

Table 2. Assumed random and systematic uncertainties. It is assumed that 80 % of the values listed in the table below correspond to random uncertainties and 20 % to systematic uncertainties (except for spectroscopy that is assumed to be 100 % systematic).

Source	Uncertainty
Baseline/continuum (offset and channelling)	0.1 %
Instrumental lines shape (modulation efficiency and phase error)	1 % and 0.01 rad
Line of sight	0.001 rad
Solar lines (intensity and spectral scale)	1 % and 1.0×10^{-6}
Temperature	1.0 K (trop)/2.0 K (strat)
Spectroscopy (intensity strength and pressure broadening – γ air)	2 % and 5 %

3.3.3 Directly retrieved tropospheric column-averaged CH_4 dry air mole fraction ($troXCH_{4_{retr}}$)

The retrieval code PROFFIT is able to perform profile inversion and we can directly retrieve tropospheric CH_4 concentration profiles from the measured spectra. We use the retrieved concentration profiles to obtain a tropospheric column-averaged CH_4 mole fraction directly from the measured spectra ($troXCH_{4_{retr}}$). Therefore, we average the retrieved CH_4 volume mixing ratios between Izaña ground level and an altitude of 6.5 km. The values retrieved at these altitudes are very sensitive to free tropospheric CH_4 and are not affected by stratospheric CH_4 (see also next Sect. 3.4.2).

3.4 Characteristics of the FTIR CH_4 data

3.4.1 Error estimation

The error calculations presented here apply the error estimation capability incorporated in the PROFFIT retrieval algorithm. This computationally efficient implementation allows performing a reasonably complete estimate of the total error budget for each individual measurement. It is based on the analytic error estimation approach of Rodgers (2000). We assume the uncertainty sources as listed in Table 2. To avoid a too optimistic systematic error budget, both a statistical as well as a systematical contribution are allowed for each error source. We assume that 80 % of the uncertainties are random and 20 % systematic, respectively. Exceptions are the spectroscopic line parameter uncertainty (line strength and pressure broadening), which is assumed to be purely systematic, and the error due to spectral measurement noise, which is assumed to be purely statistical.

The estimated random and systematic errors for the scaling retrieval are listed in Table 3. While the uncertainty in the spectroscopic parameter determines the systematic error, the baseline/continuum uncertainty is dominating the random error sources listed in Table 2.

Table 3. Errors for each parameter for the scaling retrieval for CH_4 total column.

	Statistic error (%)	Systematic error (%)
Baseline/continuum	0.23	6×10^{-3}
Instrumental lines shape	0.03	7×10^{-3}
Line of sight	0.06	7×10^{-3}
Solar lines	0.02	4×10^{-3}
Temperature	0.11	0.03
Measurement noise	0.08	
Smoothing error	0.43	
Spectroscopy		3.59
Total error	0.51	3.59

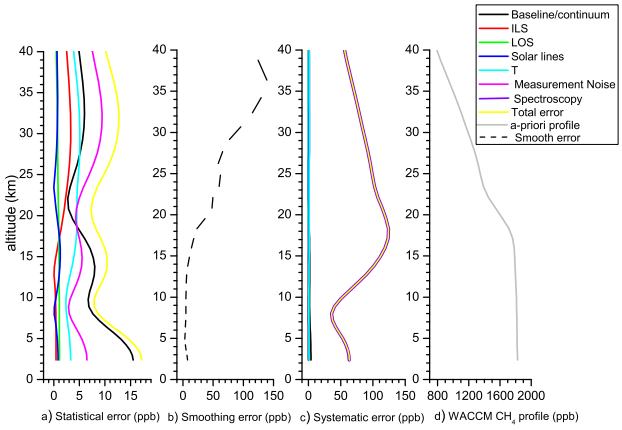

Fig. 3. Estimated errors for the profiling retrieval (PR): **(a)** statistical (random) errors of parameters listed in Table 2, **(b)** smoothing error, **(c)** systematic errors, and **(d)** climatologic CH_4 profile simulated by the WACCM model that is used as the a-priori profile. The different colours are for the different uncertainty sources as explained in the legend. The yellow line represents the total errors, and the grey line is the WACCM profile.

In addition to these parameter errors, we have to consider errors caused by the variability in the CH_4 profile shape. Generally, the shape of the actual atmospheric CH_4 will differ from the shape of the scaled WACCM CH_4 profile. This gives rise to so-called smoothing error, which can be calculated as $(\mathbf{I}-\mathbf{A})\,\mathbf{S}_a(\mathbf{I}-\mathbf{A})^T$. Here, $\mathbf{I}$ is a unity matrix, $\mathbf{A}$ is the averaging kernel, and $\mathbf{S}_a$ the assumed a priori covariance of atmospheric CH_4. Here, we use a $\mathbf{S}_a$ matrix that is obtained from the WACCM simulations. We find that the smoothing error is by far the leading random error and thus determines the precision of $totXCH_4$ produced by the scaling retrieval. When considering the smoothing error, we estimate an overall precision of about 0.51 %.

The estimated random and systematic errors for the profile retrieval are shown in Fig. 3a–c respectively. Figure 3d shows the WACCM a priori CH_4 profile in order to have a reference. We observe that in the troposphere the random errors are dominated by instrumental specific uncertainty sources: the baseline offset uncertainty and the measurement noise. The total estimated random error due to parameter uncertainties is depicted as yellow line in Fig. 3a. It is about 17 ppb (0.9 % with respect to the WACCM profile) in the lower troposphere and about 10 ppb (0.7 %) in the UT/LS region. In the stratosphere the smoothing error becomes the leading random error component.

Concerning systematic errors, spectroscopic parameters are the dominating uncertainty sources. The estimated total systematic error is depicted as yellow line in Fig. 3c. It is about 65 ppb (3.6 %) and 100 ppb (7.1 %) for the lower troposphere and the UT/LS region, respectively.

Table 4 collects the total systematic and random errors for our total XCH_4 product ($totXCH_4$) and the a posteriori-calculated tropospheric XCH_4 ($troXCH_{4_{post}}$) as obtained from the scaling retrieval (SR). Furthermore, it shows the errors for the directly retrieved tropospheric XCH_4 ($troXCH_{4_{retr}}$) and $totXCH_4$ obtained from the profile retrieval (PR). For these calculations, we assume the following uncertainties: 0.3 hPa for the surface pressure, 2.7 % for the HF column (Schneider et al., 2005), 1 % for the H_2O column (Schneider et al., 2010a), and 10 % for the b-value.

Theoretically, the scaling retrieval produces total column-averaged CH_4 ($totXCH_4$) and a posteriori-corrected tropospheric column-averaged CH_4 ($troXCH_{4_{post}}$) with a precision of 0.51 % and 0.61 %, respectively (square root of the square sum of the smoothing error, measurement noise and the statistical error). By applying a profiling retrieval, we can significantly reduce the smoothing error, which theoretically improves the precision of $totXCH_4$ to 0.41 %. The directly retrieved tropospheric column-averaged CH_4 ($troXCH_{4_{retr}}$) has an estimated precision of 0.91 %. Please note that the precision estimate for the a posteriori- calculated tropospheric XCH_4 ($troXCH_{4_{post}}$) is very likely too optimistic since we assume an uncertainty of the b-value applied in Eq. (3) of only 10 %, whereas the model-deduced HF-CH_4 correlation might be afflicted with a larger uncertainty.

3.4.2 Characteristics of the retrieved CH_4 profiles

When retrieving vertical profiles, it is important to document the vertical resolution that can be achieved with the remote sensing system. The vertical information contained in the FTIR profile is characterized by the averaging kernel matrix ($\mathbf{A}$). This matrix depends on the retrieved parameters, the quality of the measurement (the signal to noise ratio), the spectral resolution, the solar zenith angle, etc. The averaging kernel matrix describes the smoothing of the real vertical distribution of the absorber by the FTIR measurements process. Figure 4 shows the rows of a typical averaging kernel matrix of our CH_4 retrieval. The row kernels indicate the altitude regions that mainly contribute to the retrieved state. The first atmospheric levels (from Izaña ground level up to 6.5 km) are highlighted by red colour showing that, for the

Table 4. Total errors estimated for typical measurement conditions (16 June 2010).

		Typical value	Smoothing error		Statistic error		Systematic error	
		ppb	%	ppb	%	ppb	%	ppb
SR	$totXCH_4$	1743	0.43	7.50	0.27	4.71	3.50	61.01
SR*	$troXCH_{4_{post}}$	1810	0.43	7.78	0.43	7.87	3.38	61.26
PR	$totXCH_4$	1743	0.06	1.05	0.41	7.15	2.23	38.87
PR	$troXCH_{4_{retr}}$	1812	0.20	3.62	0.89	15.95	3.26	59.07

SR: scale retrieval; PR: profile retrieval; SR*: applying HF correction using the CH_4 total column from SR.

Table 5. Statistics of the daily mean comparisons between the side-by-side measuring instruments 120M and 125HR.

		N	*R*	MRD (%)	STD (%)	SF ± SEM
SR	$totXCH_4$	17	0.91	−0.17	0.28	0.9983 ± 0.0014
SR*	$troXCH_{4_{post}}$	17	0.73	−0.14	0.27	0.9986 ± 0.0014
PR	$totXCH_4$	17	0.73	−0.10	0.30	0.9990 ± 0.0015
PR	$troXCH_{4_{retr}}$	17	0.83	0.06	0.51	1.0006 ± 0.0025

N: number of data points; *R*: correlation coefficient; MRD: mean relative difference (120M – 125HR)/125HR; STD: standard deviation; SF: scaling factor (120M/125HR); SEM: standard error of the mean of the scaling factor = 2 × STD/sqrt(*N*); SR: scale retrieval; PR: profile retrieval; SR*: applying HF correction using the CH_4 total column from SR.

CH_4 mole fractions retrieved at these altitudes, there is no significant contribution from the stratosphere. The respective mixing ratios are very representative of the free troposphere, and we calculate our $troXCH_{4_{retr}}$ as the average of the mole fractions at these altitudes. With the green colour, we highlight the row kernel for an altitude of 21 km. We observe that the mole fractions values retrieved at 21 km well reflect the upper troposphere/lower stratosphere (UT/LS) region.

The trace of the averaging kernel matrix can be interpreted as the degree of freedom (DOF) of the measurement. The higher the value, the more information is obtained from the measurement. A typical DOF value obtained for our CH_4 retrieval is 2.5.

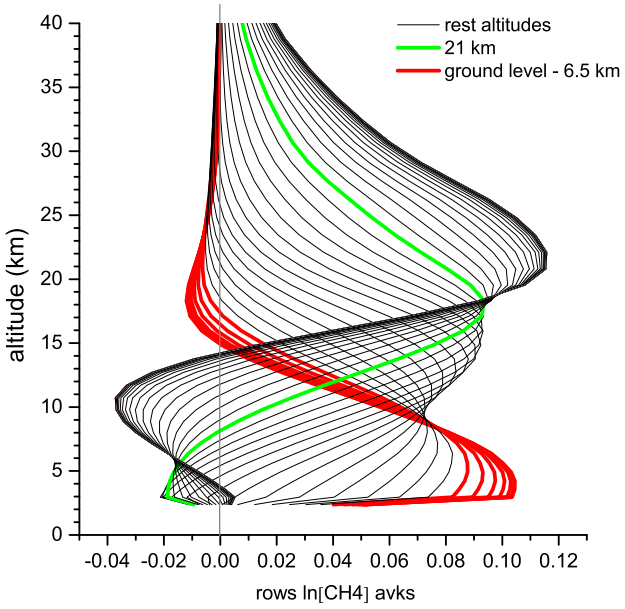

Fig. 4. Typical row averaging kernels for profiling retrieval (PR): red lines show the kernels between Izaña ground level and 6.5 km, while the green line shows the kernel corresponding to an altitude of 21 km.

4 Empirical validation

4.1 Intercomparison between the Bruker spectrometers IFS 120M and IFS 125HR

The Bruker spectrometers IFS 120M and IFS 125HR were operated side-by-side during March–April of 2005. On 17 days both instruments measured in coincidence and we can use these periods for empirically documenting the errors caused by instrument specific random uncertainties. In case of the profile retrieval, such instrument-specific random uncertainties (baseline offset and measurement noise) dominate the total random error and we can use the side-by-side instrument intercomparison as an empirical validation of the overall precision. Table 5 shows statistics of the intercomparison of the different CH_4 products obtained from the scaling and the profile retrieval. Concerning the profile retrieval (marked as PR), we find scatter values of 0.3 % for $totXCH_4$ and 0.5 % for $troXCH_{4_{retr}}$, thereby empirically documenting the good precision of these data. Concerning the scaling retrieval (marked as SR), the scatter values are even smaller; however, it is important to note that in this case the smoothing error cancels out, since it is very similar for both instruments.

4.2 FTIR versus surface in-situ GAW data

As already mentioned in Sect. 2.1, the in-situ nighttime data are very representative of free troposphere background conditions. Therefore, we compare the average of two consecutive in-situ nighttime means with the mean of the FTIR data obtained during the enclosed day. We limit this study to the 2001–2010 period, since in 1999–2000 we find an inconsistency in the surface pressure data. Due to this inconsistency,

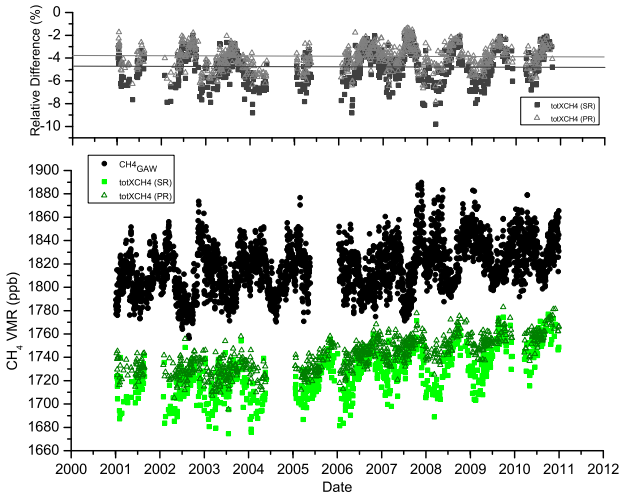

Fig. 5. $CH_{4_{GAW}}$ in-situ (black circles) and totXCH$_4$ FTIR data obtained from scaling (squares) and profiling (triangles) retrieval, respectively. Bottom panel: 2001–2010 time series for all available data; top panel: time series of the difference expressed as (FTIR − GAW)/GAW for the scaling (squares) and profiling (triangles) retrieval, respectively. The solid lines represent the mean relative difference for the scaling and profiling retrieval, respectively.

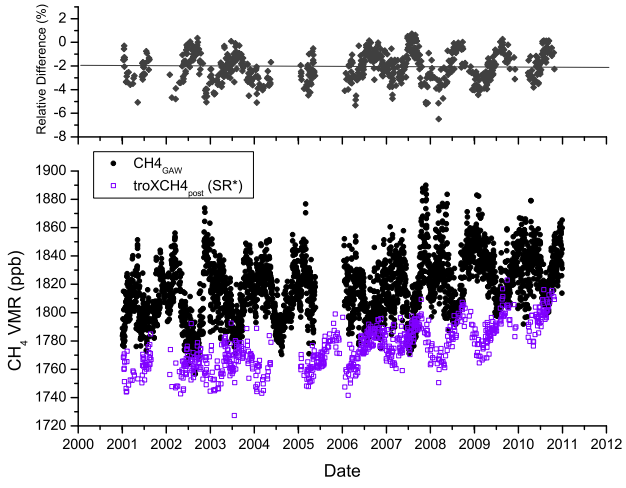

Fig. 6. Same as Fig. 5, but for the a posteriori-corrected tropospheric XCH$_4$ calculated from the total CH_4 column obtained from the scaling retrieval and applying the HF correction (troXCH$_{4_{post}}$, violet empty squares).

we are not able to calculate consistent DPC values for the 1999–2000 period (for more details see Appendix B).

The lower panel of Fig. 5 shows the daily means for totXCH$_4$ (dark green open triangles for the profiling retrieval, PR, and green solid squares for the scaling retrieval, SR) and GAW CH_4 in-situ values (black points). The upper panel depicts the relative difference between FTIR and GAW data ((FTIR − GAW)/GAW, grey open triangles for PR and dark grey solid squares for SR). For the scaling retrieval, we find a mean and standard deviation of the difference of $-4.69\,\% \pm 1.42\,\%$. The FTIR/GAW scaling factor is 0.9531. We find no significant correlation between the FTIR and GAW data (Correlation coefficient $R = 0.09$). In order to reduce the scatter caused by comparing different air masses (we compare nighttime with daytime data), we perform an additional comparison of monthly mean data (graphic not shown). There, the difference between the FTIR and GAW data is $-5.05\,\% \pm 1.28\,\%$, and the scaling factor 0.9495. Using monthly averages instead of daily mean data does not significantly reduce scatter and the bias between the two data sets. For the profiling retrieval, we find a better agreement: mean and scatter of $-3.90\,\% \pm 1.06\,\%$ and $-4.17\,\% \pm 0.92\,\%$ for daily and monthly mean differences, respectively. The FTIR/GAW scaling factor is 0.9610 (daily mean). The results of this daily and monthly mean intercomparison between the GAW data and the FTIR products are collected in Tables 6 and 7.

The lower panel of Fig. 6 shows daily means GAW data (black circles) and the troXCH$_{4_{post}}$ data (violet open squares) obtained by applying the b-value determined from the HF and CH_4 climatology of ACE-FTS ($b = -743$; see Appendix A). In the upper panel, the relative FTIR-GAW difference is shown. We obtain a mean difference and scatter of $-2.01\,\% \pm 1.24\,\%$ (FTIR/GAW scaling factor of 0.9799). The correlation plot provides a rather low correlation coefficient of 0.22 (see Table 6). For the monthly mean comparison, there is no significant change: correlation coefficient (0.15) and the relative FTIR-GAW scatter decrease to 1.19 % (see Table 7). In addition, we calculate the troXCH$_{4_{post}}$ data by applying a set of different b-values obtained by different approaches. We find that the different troXCH$_{4_{post}}$ calculations do not significantly affect the level of agreement with the GAW data (for a detailed discussion please refer to Appendix A).

Table 6. Statistics of the daily mean comparisons between the FTIR products (totXCH$_4$, troXCH$_{4_{post}}$, and troXCH$_{4_{retr}}$) and the GAW data for the period 2001–2010.

	FTIR product	N	R	MRD (%)	STD (%)	SF ± SEM
SR	totXCH$_4$	709	0.09	−4.69	1.42	0.9531 ± 0.0011
SR*	troXCH$_{4_{post}}$	709	0.22	−2.01	1.24	0.9799 ± 0.0009
PR	totXCH$_4$	709	0.39	−3.90	1.06	0.9610 ± 0.0008
PR	troXCH$_{4_{retr}}$	709	0.60	−0.13	0.97	0.9987 ± 0.0007

N: number of data points; R: correlation coefficient; MRD: mean relative difference (FTIR − GAW)/GAW; STD: standard deviation; SF: scaling factor (FTIR/GAW); SEM: standard error of the mean of the scaling factor = 2 × STD/sqrt(N); SR: scale retrieval; PR: profile retrieval; SR*: applying HF correction using the CH_4 total column from SR.

The NDACC mid-infrared spectra contain sufficient information to retrieve a CH_4 concentration profile with the characteristics that are described by the averaging kernels of Fig. 4. Theoretically, we should be able to distinguish tropospheric from stratospheric CH_4. Figure 7 shows a time series of the CH_4 profiles retrieved from the FTIR measurements

Table 7. Same as Table 6 but for monthly means.

	FTIR product	N	R	MRD (%)	STD (%)	SF ± SEM
SR	$totXCH_4$	98	0.09	−5.05	1.28	0.9495 ± 0.0026
SR*	$troXCH_{4_{post}}$	98	0.15	−2.22	1.19	0.9778 ± 0.0024
PR	$totXCH_4$	98	0.40	−4.17	0.92	0.9583 ± 0.0019
PR	$troXCH_{4_{retr}}$	98	0.69	−0.32	0.69	0.9968 ± 0.0014

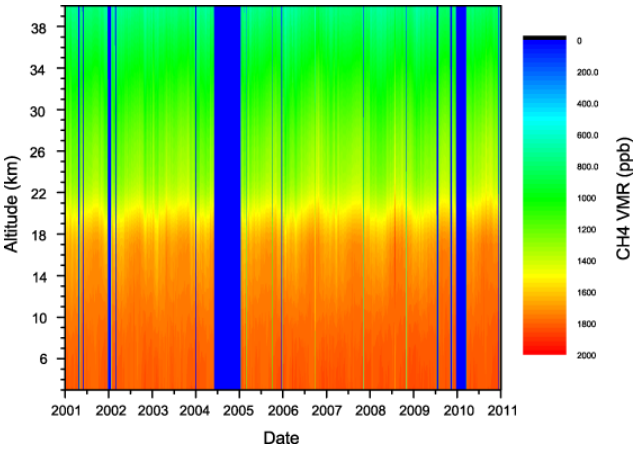

Fig. 7. Retrieved CH_4 profile time series for the period 2001–2010.

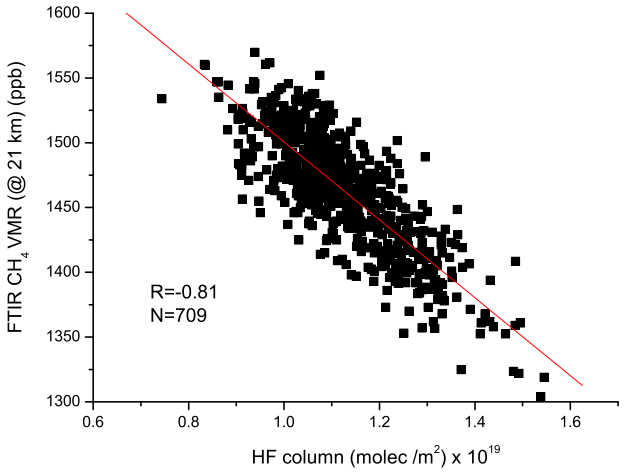

Fig. 8. Correlation plot of the retrieved total HF column versus CH_4 VMR in the UT/LS region (at 21 km). The red line shows the linear regression line.

between 2001 and 2010. CH_4 concentrations are high in the troposphere and significantly decrease in the stratosphere where CH_4 is effectively destroyed by reaction with OH, Cl, and O(^{1}D). In the CH_4 profile time series, we can clearly observe the upward shift of the UT/LS region during the summer months: in winter above 18 km, the CH_4 concentrations are typically smaller than 1600 ppb, whereas in summer 1600 ppb are still achieved at an altitude of 20 km. Vice versa to CH_4, the HF concentrations are very small in the troposphere and start to increase significantly as function of altitude in the stratosphere (HF is produced in the stratosphere by photolysis of CFCs). Similar to CH_4 in the UT/LS region, the total column of HF is a good indicator for the stratospheric contribution. Indeed, we observe a strong anti-correlation between the HF amounts and the CH_4 mixing ratio at 21 km (altitude that is very representative for the UT/LS region; see Sect. 3.4.2). This strong anti-correlation ($R = -0.81$, see Fig. 8) confirms the good quality of the CH_4 concentration retrieved for the UT/LS region.

The lower panel of Fig. 9 depicts the $troXCH_{4_{retr}}$ time series (red stars) and in black circles the daily means GAW data. The upper panel depicts the respective relative FTIR-GAW difference. We get a mean and scatter of −0.13 % ± 0.97 % and a correlation coefficient of 0.60. For the monthly mean comparison, the correlation further improves (coefficient of 0.69) and the relative FTIR-GAW scatter decreases to 0.69 % (see Tables 6 and 7). The good correlation between the GAW data and the tropospheric FTIR CH_4 concentrations, on the one hand, and the strong anti-correlation between the HF columns and the UT/LS FTIR CH_4 concentrations document the good quality of the retrieved CH_4 profiles. The NDACC FTIR systems allow measuring tropospheric CH_4 independently from stratospheric CH_4. Furthermore, the FTIR/GAW scaling factor for $troXCH_{4_{retr}}$ is very close to unity (it is 0.9987, see Table 6) indicating that the applied CH_4 HITRAN 2008 line strength parameters are in good absolute agreement to the GAW CH_4 measurements. The $troXCH_{4_{retr}}$ and the GAW datasets are consistent and could be used in a synergetic manner in flux inversion models.

Figure 10 shows the $troXCH_{4_{retr}}$/<SF> versus $CH_{4_{GAW}}$ (being <SF> the mean scaling factor between $troXCH_{4_{retr}}$ and $CH_{4_{GAW}}$). We observe that the slope of the linear regression line is smaller than unity: the fitted linear function goes from 20 ppb above the diagonal to 20 ppb below the diagonal. This is in agreement with the column sensitivity of the FTIR retrieval being smaller than 1.0 in the lower part of the troposphere (∼0.8; graphic not shown), i.e. the FTIR system does not capture the whole CH_4 variation. However, Fig. 10 might also suggest that the $troXCH_{4_{retr}}$ and the GAW datasets are not fully equivalent, because the former applies for the tropospheric column, whereas the latter applies only for the lower part of the free troposphere. The CH_4 variability might be larger in the lower part of the free troposphere than in the upper part of the free troposphere.

4.3 Interannual trend

We analyzed the CH_4 interannual trend for the FTIR and surface in-situ values. For estimating the interannual trend, we calculate yearly mean data. However, since sampling is not uniform and there might be years with more measurements than usual during a certain season, we have to subtract the

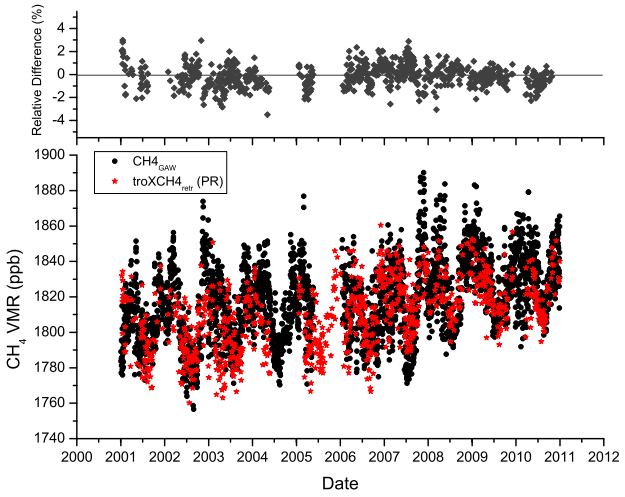

Fig. 9. Same as Fig. 5, but for the directly retrieved tropospheric XCH_4 ($troXCH_{4_{retr}}$, red stars) from the profile retrieval.

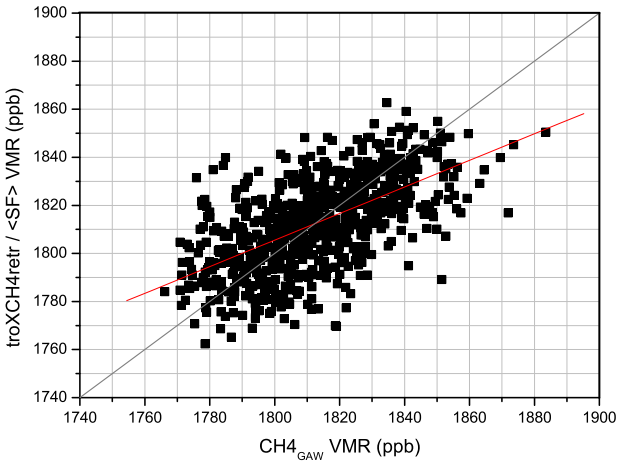

Fig. 10. $CH_{4_{GAW}}$ in-situ versus $troXCH_{4_{retr}}$/<SF> correlation plot. <SF> is the mean scaling factor between both quantities. The red line shows the linear regression line, while the grey one shows the diagonal as a reference.

annual cycle (de-seasonalise the time series). We estimate the annual cycle by fitting the following function to the time series:

$$f(t) = a_1 + a_2 t + \sum_{i=1}^{4} [b_i \cos(w_i t) + c_i \sin(w_i t)] + \sum_{j=1}^{2} [d_j \cos(k_j t) + e_j \sin(k_j t)] \quad (5)$$

where t is the time in days; a_1, a_2, b_i and c_i are the parameters of the interannual trend and d_j and e_j are the parameters of the annual cycle, all of them to be determined; $w_i = 2\pi i / N$ with N equal to the number of days in the considered period and $k_j = 2\pi j / T$ with $T = 365.25$ days. The de-seasonalised time series can then be used to calculate the yearly mean time series. The yearly mean time series of $CH_{4_{GAW}}$ and of the different FTIR products are shown in Fig. 11: in Fig. 11a for $totXCH_4$ from the scaling retrieval (SR) and the profiling retrieval (PR) and in Fig. 11b for the $troXCH_4$ products. Beside $troXCH_{4_{post}}$ and $troXCH_{4_{retr}}$, we show here $troXCH_{4_{retr\_gbm}}$, which is the same as $troXCH_{4_{retr}}$ but applying the spectral microwindows, retrieval settings and line lists recommended by Sussmann et al. (2011). For all datasets we observe that before 2005 the CH_4 concentrations remained stable and after 2005 there has been a continuous CH_4 increase. Although a detailed discussion of this trend is beyond the scope of this paper, we would like to mention that our results are in excellent agreement with those of Dlugokencky et al. (2009) and Rigby et al. (2008).

In order to assess how the yearly mean time series of the different FTIR products agree with the corresponding GAW time series, we calculate the random mean square between the yearly mean GAW data and the yearly mean FTIR data. The results are collected in Table 8. The different FTIR products agree similarly well with the GAW data.

In Table 9 we collect the change in mean CH_4 VMR between the 2001–2003 and the 2008–2010 period. The GAW concentrations ($CH_{4_{GAW}}$) changed by about 20 ppb. This change is slightly overestimated by all the FTIR data products. However, this overestimation is not significant. It is within the 1σ uncertainty range. We find that the directly retrieved tropospheric column-averaged CH_4 shows the best agreement with the GAW dataset.

4.4 De-trended CH_4 annual cycle

We compare the annual CH_4 cycles of the GAW data and of the different FTIR CH_4 products. Therefore, we de-trend the CH_4 time series. This de-trending is performed by removing the interannual trends as depicted in Fig. 11. Figure 12 shows the de-trended monthly means calculated for the 2001–2010 period: black circles for the GAW data, green solid squares and dark green open triangles for $totXCH_4$ obtained from the scaling and profiling retrieval, respectively (see Fig. 12a), violet open squares for $troXCH_{4_{post}}$, red stars for $troXCH_{4_{retr}}$, and dark yellow open stars for $troXCH_{4_{retr\_gbm}}$. All the annual cycles have been centered to zero.

We observe that $totXCH_4$ does not reproduce the tropospheric surface in-situ CH_4 variability. It is obvious that $totXCH_4$ is not a good proxy for the tropospheric seasonal CH_4 variability. Instead, the $totXCH_4$ annual variability is dominated by the annual variability of the tropopause height, which is lowest by the end of winter and continuously increases during summer. The $totXCH_4$ cycle obtained from the scaling retrieval differs significantly from the $totXCH_4$ cycle obtained from the profile retrieval. This implies that the smoothing error – which is very important for a scaling

Table 8. Root mean square (RMS) between the annual means (2001–2010 period) of GAW and the FTIR data (see Fig. 10).

	$CH_{4_{GAW}}$-*a*				
a	$totXCH_4$ (SR)	$totXCH_4$ (PR)	$troXCH_{4_{post}}$ (SR*)	$troXCH_{4_{retr}}$ (PR)	$troXCH_{4_{retr\_gbm}}$ (PR)
RMS [ppb]	5.15	4.52	4.54	4.81	7.51

SR: scale retrieval; PR: profile retrieval; SR*: applying HF correction using the CH_4 total column from SR.

Table 9. Difference between the mean CH_4 VMR in 2001–2003 and in 2008–2010 with its associated 1σ uncertainty.

Dataset	$CH_{4_{GAW}}$	$totXCH_4$ (SR)	$totXCH_4$ (PR)	$troXCH_{4_{post}}$ (SR*)	$troXCH_{4_{retr}}$ (PR)	$troXCH_{4_{retr\_gbm}}$ (PR)
Difference [ppb]	19.65 $\pm$5.00	26.46 $\pm$9.19	25.61 $\pm$4.74	26.97 $\pm$7.71	22.79 $\pm$5.12	26.79 $\pm$4.91

SR: scale retrieval; PR: profile retrieval; SR*: applying HF correction using the CH_4 total column from SR.

retrieval with fixed first guess profile shape – depends on the season.

As with the $totXCH_4$ cycle, the $troXCH_{4_{post}}$ cycle does not capture the minimum during summer and the maximum in the early winter. Instead, it follows more or less the annual cycle of the tropopause altitude. We observe that the a posteriori correction method as applied here does not adequately account for the stratospheric contribution.

By comparison, the $troXCH_{4_{retr}}$ cycle is more consistent with the GAW in-situ cycle. The amplitudes and phases of both cycles are very similar, thereby confirming that the directly retrieved tropospheric column-averaged XCH_4 values are a very good proxy for the free tropospheric CH_4 concentrations.

We find that the $troXCH_{4_{retr\_gbm}}$ cycle does not reconstruct the GAW in-situ cycle as well as does $troXCH_{4_{retr}}$. The $troXCH_{4_{retr\_gbm}}$ retrieval was optimised for retrievals of total column-averaged XCH_4 from a range of sites and water vapour amounts, not tropospheric column-averaged XCH_4. The difference is presumed to be due to different treatment of water vapour and the use of different line lists for CH_4.

5 Remark on non-transferability to the near-infrared spectra

In our work we investigate CH_4 retrievals by applying the NDACC high- resolution mid-infrared solar absorption spectra (typical spectral resolution is $0.005\,cm^{-1}$). We find that the HF correction method based on a simple scaling retrieval of a climatologic CH_4 profile does not work sufficiently well when applying the high-resolution mid-infrared NDACC spectra. In Appendix A we document that the problem is not the b-value but the limited precision of the CH_4 total column amount that is achieved by a simple scaling retrieval. In addition to NDACC, the ground-based FTIR network TCCON has been established during the last few years. Within TCCON, spectra are measured in the near-infrared spectral region at a spectral resolution of $0.02\,cm^{-1}$. It is important to remark that our results about the HF correction method found for the mid-infrared spectra cannot be transferred in a straightforward manner to the near-infrared TCCON retrievals. There are some important differences:

1. In the high-resolution mid-infrared NDACC spectra, we can well observe the pressure broadening effect, i.e. these spectra contain a lot of information about the vertical distribution of the CH_4 molecules. As a consequence for NDACC, a CH_4 profile retrieval is more feasible. A simple scaling retrieval will produce less precise CH_4 total column amounts. The situation is different for the near-infrared TCCON spectra. There, the CH_4 signatures are less sensitive to the vertical distribution of CH_4. First, in the near-infrared spectra, the Doppler core is more important than in the mid-infrared spectra (pressure broadening is more difficult to observe), and second, the spectral resolution of TCCON spectra is significantly lower than the one of the NDACC spectra. Consequently, in the near-infrared TCCON, a profile retrieval may have only small or negligible benefit and a scaling retrieval may produce equally precise and accurate column amounts.

2. The TCCON near-infrared observations have the great advantage that the observed air mass can be monitored by analyzing O_2 absorption signatures. Since atmospheric O_2 amounts are very stable, one can use the CH_4/O_2 ratio as a measure of the column-averaged CH_4 amount. Thereby, the measurement is a relative measurement and TCCON CH_4 columns are theoretically very precise.

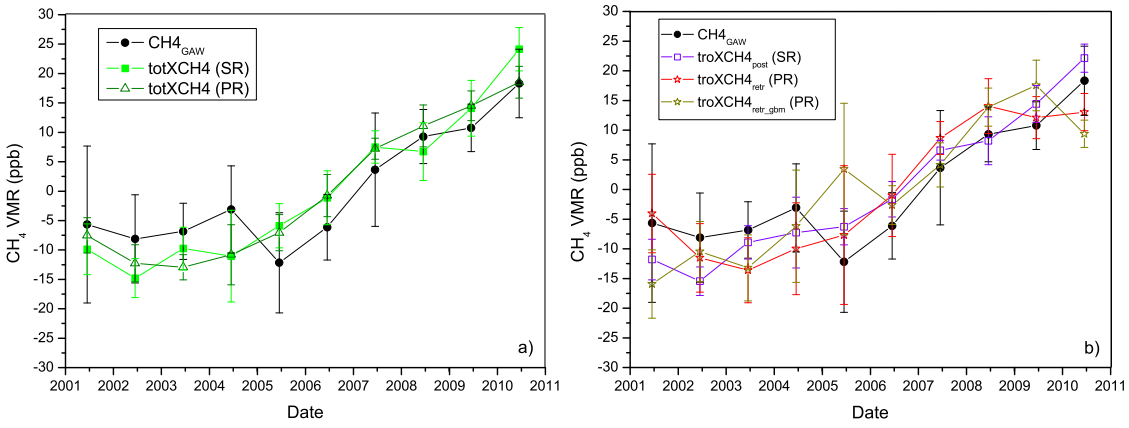

Fig. 11. Annual mean for the $CH4_{GAW}$ in-situ (black dots) and the different FTIR products considering coincident data and centered at zero. **(a)** total XCH_4 products: green squares for $totXCH_4$ from SR, and green dark open triangles for $totXCH_4$ from PR; **(b)** tropospheric XCH_4 products: violet open squares for $troXCH4_{post}$, red stars for $troXCH4_{retr}$, and open dark yellow stars for $troXCH4_{retr\_gbm}$. The error bars correspond to the standard error of the mean [$2 \times$ STD/sqrt(N)].

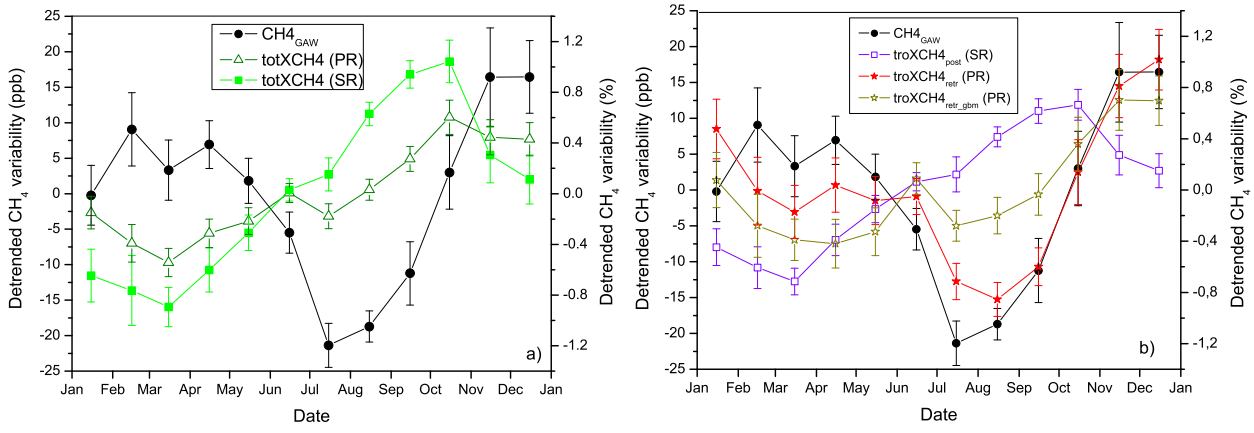

Fig. 12. The multi-annual mean annual cycles derived for data of the 2001–2010 period for the different $CH4_{GAW}$ (black dots) and the different FTIR products: **(a)** total XCH_4 products; green squares for SR and green dark open triangles for PR; **(b)** tropospheric XCH_4 products: violet open squares for $troXCH4_{post}$, red stars for $troXCH4_{retr}$ and open dark yellow stars for $troXCH4_{retr\_gbm}$. The error bars correspond to the standard error of the mean [2 x STD/sqrt(N)].

6 Outlook and conclusions

In the framework of the NDACC, ground-based FTIR experiments have recorded high-resolution mid-infrared solar absorption spectra for more than a decade at about 15 globally distributed sites. We examine two different CH_4 retrieval principles: first, a simple scaling of a fixed climatologic profile and, second, a CH_4 profile retrieval.

A scaling retrieval is indicated if there is no significant variation in the profile shape or if the variations in the profile shape are not reflected in the measured solar absorption spectra (e.g. due to limited spectral resolution or measurement noise). However, our study shows that the high quality NDACC spectra contain significant information about the typical vertical variability of CH_4 converting the smoothing error in the leads error component of the scaling retrieval. We estimate a theoretical precision of the total XCH_4 of 0.51 %. The smoothing error of total XCH_4 can be significantly reduced if performing a profile retrieval leading to an improved precision of 0.41 %. This good precision is empirically confirmed by a side-by-side intercomparison study applying two FTIR instruments in 2005. We document that only the profile retrieval produces total XCH_4 with high precision and should be used for producing data for scientific applications. We find, for instance, the annual XCH_4 cycle obtained by the scaling retrieval significantly differs from the cycle obtained by the profile retrieval.

While precise total XCH_4 FTIR data are an important reference for the validation of space-base XCH_4 experiments (e.g. SCIAMACHY, GOSAT, OCO-2), the total XCH_4

amounts are significantly affected by the variability of the stratospheric CH_4 contribution. We document that the annual cycle of total XCH_4 rather follows the annual cycle of the tropopause altitude and not the annual cycle of tropospheric CH_4 mole fraction. Our study shows that total XCH_4 is no valid proxy for tropospheric CH_4.

We investigate two methods for obtaining a tropospheric CH_4 proxy from the FTIR measurements. First, the often applied a posteriori correction method, which applies a CH_4 scaling retrieval and a posteriori corrects the stratospheric CH_4 contribution using HF total column amounts as stratospheric CH_4 proxy. This data set is called $troXCH4_{post}$ throughout the paper. Second, we directly retrieve tropospheric column-averaged XCH_4 amounts from the spectra applying the profile retrieval. This data set is called $troXCH4_{retr}$ throughout the paper.

Concerning $troXCH4_{post}$ we estimate a precision of 0.61 %. However, this estimation cannot be empirically confirmed by our comparison to the GAW CH_4 in-situ data (the scatter between $CH4_{GAW}$ and $troXCH4_{post}$ is as large as 1.24 %). The reason might be an underestimation of the smoothing error, a too optimistic assumption of the uncertainty of the b-value, or a seasonal variability of the fluorine partitioning. The scientific usefulness of $troXCH4_{post}$ data is rather doubtful. For instance, the data do not capture the full amplitude of the tropospheric CH_4 annual cycle.

For $troXCH4_{retr}$ we estimate a theoretical precision of 0.91 %. This value is consistent with the results of the side-by-side FTIR intercomparison study of 2005, and it is well confirmed by the comparison to the GAW CH_4 in-situ data (we obtain a scatter between $CH4_{GAW}$ and $troXCH4_{retr}$ of 0.97 %). Furthermore, we found that the FTIR/GAW scaling factor is very close to unity, suggesting that the NDACC FTIR network can provide tropospheric column-averaged CH_4 that is very consistent to the CH_4 data of the GAW in-situ network. The annual cycles of $troXCH4_{retr}$ and $CH4_{GAW}$ are very similar (phase and amplitude). For investigating the CH_4 interchange between atmosphere, biosphere, and ocean, we strongly recommend using the directly retrieved tropospheric XCH_4 instead of the tropospheric XCH_4 produced by the a posteriori correction method.

Although we do not perform a direct empirical validation of the total column-averaged XCH_4 obtained by the profile retrieval, it is important to recall that we observe, first, a good correlation of the retrieved tropospheric column-averaged XCH_4 amounts with the GAW data, and second, a good correlation of the retrieved lower stratospheric CH_4 concentrations with the HF data. These observations document the high quality of the retrieved CH_4 profile in the troposphere as well as in the stratosphere and thus strongly suggest a high quality for the total column-averaged XCH_4.

Due to its long-term characteristics, the NDACC tropospheric XCH_4 data set can make valuable contributions when investigating sources and sinks of CH_4. In our paper we exclusively investigate CH_4 retrievals applying mid-infrared NDACC spectra. In the future we plan a similar study for the near-infrared spectral region, which is recorded by the TCCON experiments. We plan to examine the practicability and benefits of a profile retrieval for obtaining highly precise total column-averaged XCH_4 amounts from TCCON spectra. Furthermore, we will use the Izaña GAW CH_4 in-situ data set for documenting the precision of possible TCCON tropospheric column-averaged CH_4 data and its level of consistency with the GAW CH_4 in-situ data.

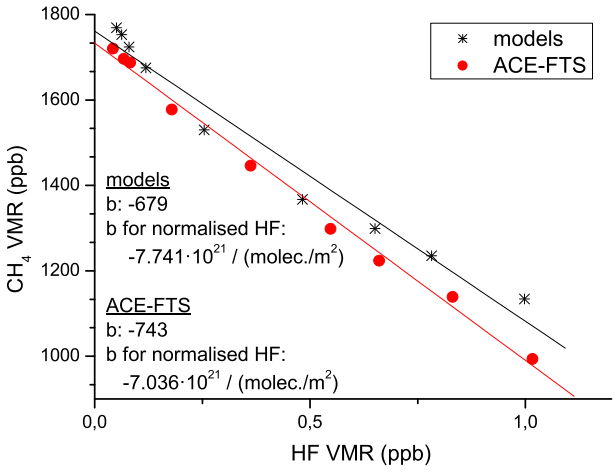

Fig. A1. HF volume mixing ratio versus CH_4 volume mixing ratio between the levels 10 and 100 hPa. The solid lines represent the regression line for models (black line) and ACE-FTS (red line). The b-values are also shown for the normalised HF profiles.

Appendix A

Using HF column amounts as proxy for the tropopause altitude

We calculate the CH_4-HF slope equilibrium (b-value) by applying three different approaches: (a) as Washenfelder et al. (2003) from the stratospheric CH_4 and HF VMR, (b) from the CH_4 and HF total columns and (c) fitting Eq. (3) (from the manuscript) but substituting the $troXCH4_{post}$ for $CH4_{GAW}$. For approaches (a) and (b) we determine the b-value by applying different datasets. We use model data (a CH_4 climatology for the 2004–2006 period from WACCM, and an HF climatology for the mid-2000s from KASIMA) as well as experimental data (a 2004–2008 climatology of CH_4 and HF profiles and for the latitude 25° N–35° N from the ACE-FTS satellite experiment; Jones et al., 2012). The three approaches give different b-values. The scatter between the different b-values can be used as the b-values uncertainty.

a. The b-value is determined by calculating the regression line between the stratospheric CH_4 and HF VMR profiles obtained from the ACE-FTS measurements

Table A1. $troCH_{4_{post}}$ calculated from $CH_{4_{col}}$ of the scaling retrieval.

Applied method to calculated the b-value	b-value	$troXCH_{4_{post}}$ vs. $CH_{4_{GAW}}$			
		R	MRD (%)	STD (%)	SF
Correlation of ACE VMRs (10 to 100 hPa)	−743	0.216	−2.01	1.24	0.9799
Correlation of ACE columns (shifts: −30 to +30 hPa)	−689	0.205	−2.21	1.25	0.9780
Correlation of modelled VMRs (10 to 100 hPa)	−679	0.203	−2.24	1.26	0.9776
Correlation of modelled columns (shifts: −30 to +30 hPa)	−901	0.247	−1.45	1.21	0.9855
fit: $CH_{4_{GAW}}$, $CH_{4_{FTIR}}$, HF_{FTIR}	−1368	0.344	0.21	1.12	1.0021

R: correlation coefficient; MRD: mean relative difference (FTIR-GAW)/GAW; STD: standard deviation; SF: scaling factor (FTIR/GAW).

Table A2. Same as Table A1 but for normalised HF time series.

Applied method to calculated the b-value	b-value $[(molec./m^2)^{-1}]$	$troXCH_{4_{post}}$ vs. $CH_{4_{GAW}}$			
		R	MRD (%)	STD (%)	SF
Correlation of ACE VMRs (10 to 100 hPa)	-7.036×10^{21}	0.193	−2.28	1.27	0.9772
Correlation of ACE columns (shifts: −30 to +30 hPa)	-6.529×10^{21}	0.185	−2.45	1.28	0.9755
Correlation of modelled VMRs (10 to 100 hPa)	-7.741×10^{21}	0.205	−2.04	1.25	0.9796
Correlation of modelled columns (shifts: −30 to +30 hPa)	-1.027×10^{22}	0.249	−1.19	1.21	0.9881
fit: $CH_{4_{GAW}}$, $CH_{4_{FTIR}}$, $HF_{FTIRnorm}$	-1.522×10^{22}	0.341	0.48	1.13	1.0048

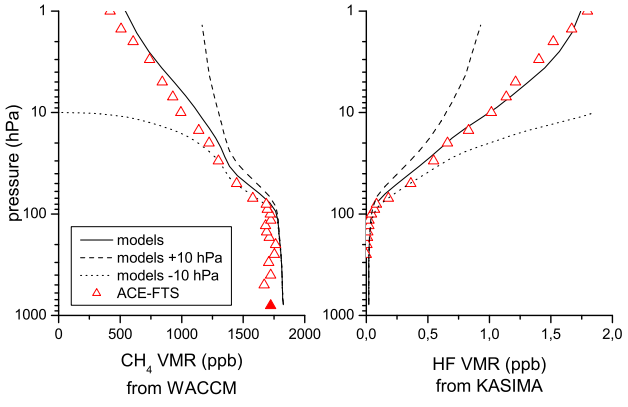

Fig. A2. Solid lines correspond to the modelled profiles for CH_4 (left panel) and HF (right panel). Dotted and dashed lines show the models mixing ratios for −10 hPa and +10 hPa vertical profile shifts, respectively. Red open triangles show the ACE-FTS mixing ratios (the red filled triangle is the CH_4 concentration that we use for the lower troposphere, where ACE-FTS is not sensitive anymore).

between the 10 and 100 hPa. We also determine a b-value from the modelled VMR profiles. The CH_4-HF correlation plots are depicted in Fig. A1. We calculate the correlations for the 10 to 100 hPa levels in agreement with Washenfelder et al. (2003), but in comparison to Washenfelder et al. (2003) we only determine one single b-value. Actually, the b-value changes with the increase of HF amounts by about 1 % per year. Consequently, using a single b-value representative for the 2004–2006/2008 time period for the whole time series (2001–2010) means an uncertainty of the b-value of up to 5 %. We obtain values of −743 and −679 for ACE-FTS profiles and models, respectively. For comparison Washenfelder et al. (2003) estimated a b-value for 1992 of about −950, which is in reasonable agreement with our b-values obtained for the mid-2000s.

In addition, we calculate a b-value from a normalised HF-profile. The normalisation means that the VMR values have been divided by the HF total column amounts. This b-value can then be applied in Eq. (3) together with a normalised HF time series. The normalisation allows using a b-value that is constant over time. We get values of $-7.036 \times 10^{21}\,(molec/m^2)^{-1}$ and $-7.741 \times 10^{21}\,(molec/m^2)^{-1}$ for ACE-FTS and models, respectively.

b. As can be seen in Fig. A1 between 10 and 100 hPa, the correlation is not perfectly linear. In particular for the model profiles assuming a linear correlation might cause an erroneous b-value. Therefore, we test an additional approach that determines the b-value from correlating CH_4 and HF total column amounts. The column amounts are calculated from profiles that are shifted vertically (between −30 hPa and +30 hPa; see Fig. A2). Figures A3 and A4 plot the correlations using ACE-FTS profiles and models

Table A3. Same as Table A1 but for $CH_{4_{col}}$ from profiling retrieval.

Applied method to calculated the b-value	b-value	troXCH$_{4_{post}}$ vs. CH$_{4_{GAW}}$			
		R	MRD (%)	STD (%)	SF
Correlation of ACE VMRs (10 to 100 hPa)	−743	0.519	−1.23	0.97	0.9877
Correlation of ACE columns (shifts: −30 to +30 hPa)	−689	0.510	−1.42	0.98	0.9858
Correlation of modelled VMRs (10 to 100 hPa)	−679	0.509	−1.45	0.98	0.9855
Correlation of modelled columns (shifts: −30 to +30 hPa)	−901	0.541	−0.67	0.96	0.9933
fit: $CH_{4_{GAW}}$, $CH_{4_{FTIR}}$, HF_{FTIR}	−1368	0.582	0.99	0.94	1.0099

Table A4. Same as Table A3 but for normalised HF time series.

Applied method to calculated the b-value	b-value [(molec./m^2)$^{-1}$]	troXCH$_{4_{post}}$ vs. CH$_{4_{GAW}}$			
		R	MRD (%)	STD (%)	SF
Correlation of ACE VMRs (10 to 100 hPa)	-7.036×10^{21}	0.499	−1.50	0.99	0.9851
Correlation of ACE columns (shifts: −30 to +30 hPa)	-6.529×10^{21}	0.492	−1.67	0.99	0.9833
Correlation of modelled VMRs (10 to 100 hPa)	-7.741×10^{21}	0.510	−1.26	0.98	0.9874
Correlation of modelled columns (shifts: −30 to +30 hPa)	-1.027×10^{22}	0.542	−0.41	0.96	0.9960
fit: $CH_{4_{GAW}}$, $CH_{4_{FTIR}}$, $HF_{FTIRnorm}$	-1.522×10^{22}	0.580	1.27	0.94	1.0130

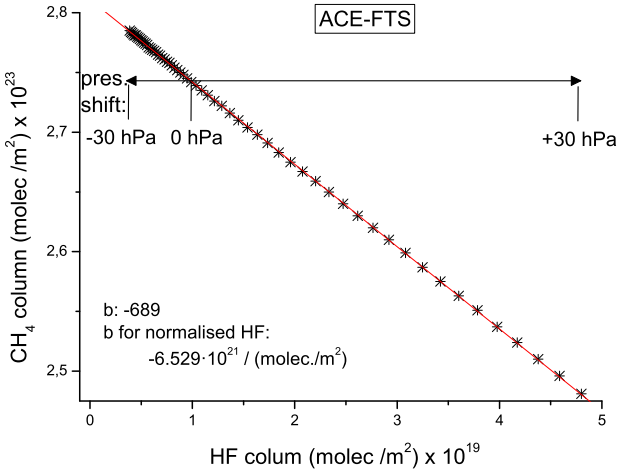

Fig. A3. Correlation plot between the CH_4 and HF total column amounts obtained for different vertical shifts of the CH_4 and HF ACE-FTS profiles.

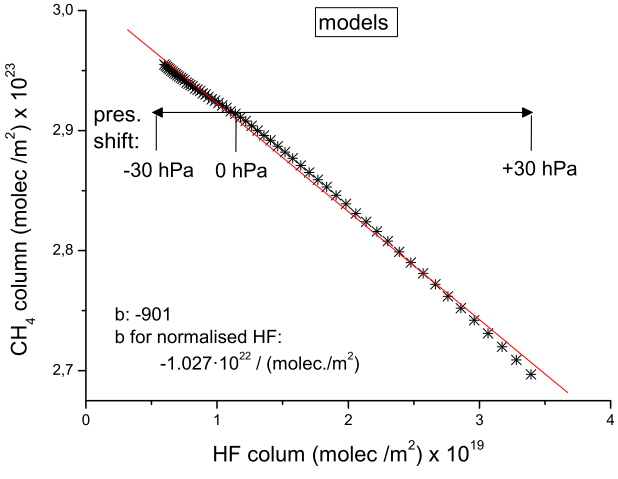

Fig. A4. Same as Fig. A3 but for model profiles.

profiles, respectively. We get b-values of −689 and −901 for ACE-FTS and models, respectively. For normalised profiles we get -6.529×10^{21} (molec/m^2)$^{-1}$ and -1.027×10^{22} (molec/m^2)$^{-1}$ for ACE-FTS and models, respectively.

c. Finally, we calculate an empirical b-value determined by fitting all the high quality data that are available at the Izaña Observatory: the FTIR CH_4 total column amounts determined from the profiling retrieval, the FTIR HF total column amounts, and the $CH_{4_{GAW}}$ data.

$$CH_{4_{col}}(t) = k \cdot \left(DPC(t) \cdot CH_{4_{GAW}}(t)\right) + b \cdot HF_{col}(t) \quad \text{(A1)}$$

The parameters b and k are obtained by least squares fit. The so-obtained b-value is the "best possible b-value". Applying this b-value in Eq. (3) produces a troXCH$_{4_{post}}$ with the best possible correlation to $CH_{4_{GAW}}$. This empirical value represents the best correction that is possible with the "HF-procedure". We get a b-value of −1368, and -1.522×10^{22} (molec/m^2)$^{-1}$ when it is applied for the normalised HF.

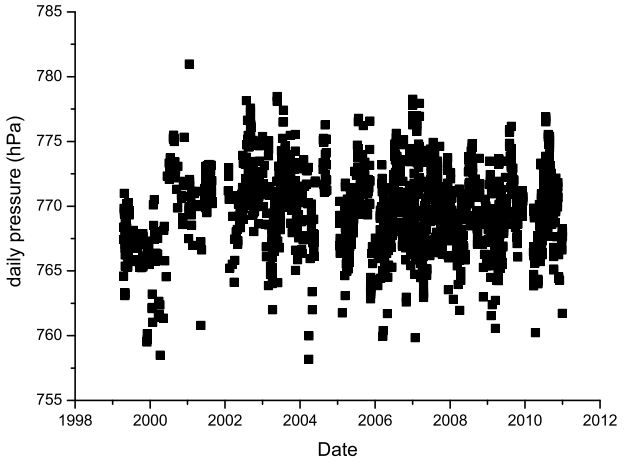

Fig. B1. Time series of the daily mean pressure at Izaña ground level.

According to Eq. (3) we calculate $troXCH4_{post}$ for the different b-values, considering the de-trended and normalised HF time series, and for CH_4 total columns obtained from the scaling retrieval. Tables A1 and A2 document the agreement between $troXCH4_{post}$ and $CH4_{GAW}$. We want to remark that the agreement between the $troXCH4_{post}$ and $CH4_{GAW}$ only slightly depends on the applied b-value. The correlation factor (R) and the standard deviation (STD) are roughly the same for the different b-values. Even for our empirical "best possible b-value", we get an agreement that is significantly poorer that the agreement between the directly retrieved tropospheric column-averaged CH_4 and $CH4_{GAW}$.

On the other hand, the agreement strongly depends on the quality of the applied CH_4 total column data. This is documented by Tables A3 and A4, which show the same as Tables A1 and A2 but using the CH_4 total column amounts obtained from the profile retrieval. These total column amounts are of higher quality than the CH_4 total column amounts obtained from the scaling retrieval (see error estimation section of the manuscript). We conclude that in the mid-infrared spectra, the leading error source of the "HF-procedure" is the uncertainty of the applied $CH4_{col}$ and not the uncertainty of the b-value.

Appendix B

Surface pressure measurements at Izaña Observatory

The 1999–2010 surface pressure measurement time series presents a jump at the beginning of 2001. The reason is that before and after 2001 two different types of pressure sensors have been applied: until 2001 a Thyas sensor ($\sim \pm 1$ hPa) and since 2001 a Setra sensor (± 0.3 hPa). Furthermore, the sensors were located at different positions and altitudes.

Figure B1 shows the time series of the daily mean pressure values acquired from both sensors at Izaña station. This jump will propagate into the $totXCH_4$ and $troXCH4_{post}$ with about 7 ppb and 8 ppb, respectively. Therefore, we decided to present CH_4 time series only from 2001 onward.

Acknowledgements. E. Sepúlveda enjoys a pre-doctoral fellowship from the Spanish Ministry of Education. M. Schneider is supported by the European Research Council under the European Community's Seventh Framework Programme (FP7/2007-2013)/ERC Grant agreement number 256961. The research leading to these results has received funding from the European Community's Seventh Framework Programme (FP7/2007-2013) within the NORS project (grant agreement no. 284421). We are grateful to the Goddard Space Flight Center for providing the temperature and pressure profiles of the National Centers for Environmental Prediction via the automailer system.

Edited by: D. Griffith

References

Bousquet, P., Ringeval, B., Pison, I., Dlugokencky, E. J., Brunke, E.-G., Carouge, C., Chevallier, F., Fortems-Cheiney, A., Frankenberg, C., Hauglustaine, D. A., Krummel, P. B., Langenfelds, R. L., Ramonet, M., Schmidt, M., Steele, L. P., Szopa, S., Yver, C., Viovy, N., and Ciais, P.: Source attribution of the changes in atmospheric methane for 2006–2008, Atmos. Chem. Phys., 11, 3689–3700, doi:10.5194/acp-11-3689-2011, 2011.

Dlugokencky, E. J., Bruhwiler, L., White, J. W. C., Emmons, L. K., Novelli, P. C., Montzka, S. A., Masarie, K. A., Lang, P. M., Crotwell, A. M., Miller, J. B., and Gatti, L. V.: Observational constraints on recent increases in the atmospheric CH_4 burden, Geophys. Res. Lett., 36, L18803, doi:10.1029/2009GL039780, 2009.

Frankenberg, C., Meirink, J. F., van Weele, M., Platt, U., and Wagner, T.: Assessing methane emissions from global spaceborne observations, Science, 308, 1010–8438, 2005.

Frankenberg, C., Aben, I., Bergamaschi, P., Dlugokencky, E. J., van Hees, R., Houweling, S., van der Meer, P., Snel, R., and Tol, P.: Global column-averaged methane mixing ratios from 2003 to 2009 as derived from SCIAMACHY: Trends and variability, J. Geophys. Res., 116, D04302, doi:10.1029/2010JD014849, 2011.

Gomez-Pelaez, A. J. and Ramos, R.: Improvements in the Carbon Dioxide and Methane Continuous Measurement Programs at Izaña Global GAW Station (Spain) during 2007–2009, Report of the 15th WMO/IAEA Meeting of Experts on Carbon Dioxide, Other Greenhouse Gases, and Related Tracer Measurement Techniques, 7–10 September 2009, GAW Report number 194, WMO TD 1553, available at: http://www.wmo.int/pages/prog/arep/gaw/gaw-reports.html (last access: 2 February 2012), Jena, Germany, 330 pp., 2011.

Gomez-Pelaez, A.J., Ramos, R., Cuevas, E., and Gomez-Trueba, V.: 25 years of continuous CO_2 and CH_4 measurements at Izaña Global GAW mountain station: annual cycles and interannual trends; Proceedings of the Symposium on Atmospheric Chemistry and Physics at Mountain Sites, ACP Symposium 2010, 8–10 June 2010, available at: http://www.izana.org/publications/

Abstract_25-year_CO2_and_CH4_Izana.pdf (last access: 2 February 2012), Interlaken, Switzerland, 157–159, 2010.

Gomez-Pelaez, A. J., Ramos, R., Gomez-Trueba, V., Campo-Hernandez, R., Dlugokencky, E., and Conway, T.: New improvements in the Izaña (Tenerife, Spain) global GAW station in-situ greenhouse gases measurement program; to be published in the proceedings of the 16th WMO/IAEA Meeting on Carbon Dioxide, Other Greenhouse Gases, and Related Measurement Techniques, 25–28 October 2011, GAW Report to be publish, Wellington, New Zealand, 2012.

Hase, F.: Inversion von Spurengas-profilen aus hochaufgelösten bodengebundenen FTIR-Messungen in Absorption, Forschungszentrum Kalrsruhe, FZKA 6512, 2000.

Hase, F.: Interactive comment on "Strategy for high-accuracy-and-precision retrieval of atmospheric methane from the mid-infrared FTIR network" by R. Sussmann et al., Atmos. Meas. Tech. Discuss., 4, C1048–C1048, 2011.

Hase, F., Blumenstock, T., and Paton-Walsh, C.: Analysis of the instrumental line shape of high-resolution Fourier transform IR spectrometers with gas cell measurements and new retrieval software, Appl. Optics, 38, 3417–3422, 1999.

Hase, F., Hannigan, J. W., Coffey, M. T., Goldman, A., Höpfner, M., Jones, N. B., Rinsland, C. P., and Wood, S. W.: Intercomparison of retrieval codes used for the analysis of high-resolution, ground-based FTIR measurements, J. Quant. Spectrosc. Ra., 87, 25–52, 2004.

IPCC: Climate Change 2007 – The Physical Science Basis: Contribution of Working Group I to the Fourth Assessment Report of the Intergovernmental Panel on Climate, Cambridge University Press, Cambridge, United Kingdom and New York, NY, USA, 2007.

Jones, A., Walker, K. A., Jin, J. J., Taylor, J. R., Boone, C. D., Bernath, P. F., Brohede, S., Manney, G. L., McLeod, S., Hughes, R., and Daffer, W. H.: Technical Note: A trace gas climatology derived from the Atmospheric Chemistry Experiment Fourier Transform Spectrometer (ACE-FTS) data set, Atmos. Chem. Phys., 12, 5207–5220, doi:10.5194/acp-12-5207-2012, 2012.

Keppler, F., Hamilton, T. G., Braß, M., and Rockmann, T.: Methane emissions from terrestrial plants under aerobic conditions, Nature, 439, 187–191, doi:10.1038/nature04420, 2006.

Olsen, S. C. and Randerson, J. T.: Differences between surface and column atmospheric CO_2 and implications for carbon cycle research, J. Geophys. Res., 109, D02301, doi:10.1029/2003JD003968, 2004.

Rigby, M., Prinn, R. G., Fraser, P. J., Simmonds, P. G., Langenfelds, R. L., Huang, J., Cunnold, D. M., Steele, L. P., Krummel, P. B., Weiss, R. F., O'Doherty, S., Salameh, P. K., Wang, H. J., Harth, C. M., M¨uhle, J., and Porter, L. W.: Renewed growth of atmospheric methane, Geophys. Res. Lett., 35, L22805, doi:10.1029/2008GL036037, 2008.

Rodgers, C. D.: Inverse Methods for Atmospheric Sounding: Theory and Praxis, World Scientific Publishing Co., Singapore, ISBN 981-02-2740-X, 2000.

Rothman, L. S., Gordon, I. E., Barbe, A., Chris Benner, D., Bernath, P. F., Birk, M., Boudon, V., Brown, L. R., Campargue, A., Champion, J.-P., Chance, K., Coudert, L. H., Dana, V., Devi, V. M., Fally, S., Flaud, J.-M., Gamache, R. R., Goldman, A., Jacquemart, D., Kleiner, I., Lacome, N., Lafferty, W. J., Mandin, J.-Y., Massie, S. T., Mikhailenko, S. N., Miller, C. E., Moazzen-Ahmadi, N., Naumenko, O. V., Nikitin, A. V., Orphal, J., Perevalov, V. I., Perrin, A., Predoi-Cross, A., Rinsland, C. P., Rotger, M., Simeckova, M., Smith, M. A. H., Sung, K., Tashkun, S. A., Tennyson, J., Toth, R. A., Vandaele, A. C., and Vander-Auwera, J.: The HITRAN 2008 molecular spectroscopic database, J. Quant. Spectrosc. Ra., 110, 533–572, doi:10.1016/j.jqsrt.2009.02.013, 2009.

Schneider, M., Blumenstock, T., Chipperfield, M. P., Hase, F., Kouker, W., Reddmann, T., Ruhnke, R., Cuevas, E., and Fischer, H.: Subtropical trace gas profiles determined by ground-based FTIR spectroscopy at Izaña (28° N, 16° W): Five-year record, error analysis, and comparison with 3-D CTMs, Atmos. Chem. Phys., 5, 153–167, doi:10.5194/acp-5-153-2005, 2005.

Schneider, M., Hase, F., and Blumenstock, T.: Water vapour profiles by ground-based FTIR spectroscopy: study for an optimised retrieval and its validation, Atmos. Chem. Phys., 6, 811–830, doi:10.5194/acp-6-811-2006, 2006.

Schneider, M., Toon, G. C., Blavier, J.-F., Hase, F., and Leblanc, T.: H_2O and δD profiles remotely-sensed from ground in different spectral infrared regions, Atmos. Meas. Tech., 3, 1599–1613, doi:10.5194/amt-3-1599-2010, 2010a.

Schneider, M., Romero, P. M., Hase, F., Blumenstock, T., Cuevas, E., and Ramos, R.: Continuous quality assessment of atmospheric water vapour measurement techniques: FTIR, Cimel, MFRSR, GPS, and Vaisala RS92, Atmos. Meas. Tech., 3, 323–338, doi:10.5194/amt-3-323-2010, 2010b.

Sussmann, R., Forster, F., Rettinger, M., and Jones, N.: Strategy for high-accuracy-and-precision retrieval of atmospheric methane from the mid-infrared FTIR network, Atmos. Meas. Tech., 4, 1943–1964, doi:10.5194/amt-4-1943-2011, 2011.

Washenfelder, R. A., Wennberg, P. O., and Toon, G. C.: Tropospheric methane retrieved from ground-based near-IR solar absorption spectra, Geophys. Res. Lett., 30, L017969, doi:10.1029/2003GL017969, 2003.

Zellweger, C., Klausen, J., and Buchmann, B.: System and performance audit for surface ozone, carbon monoxide, methane and nitrous oxide at the global GAW station Izana, Spain, March 2009, available at: http://gaw.empa.ch/audits/IZO_2009.pdf (last access: 2 February 2012), WCC-Empa Report 09/1, 2009.